International Journal of Fatigue 99 (2017) 163–174

Contents lists available at ScienceDirect

International Journal of Fatigue

journal homepage: www.elsevier.com/locate/ijfatigue

Epistemic uncertainty quantification in metal fatigue crack growth analysis using evidence theory

Hesheng Tang [a,*], Dawei Li [b], Jingjing Li [b], Songtao Xue [b]

[a] State Key Laboratory for Disaster Reduction in Civil Engineering, Tongji University, 1239, Siping Rd., Shanghai, China
[b] Research Institute of Structural Engineering and Disaster Reduction, Tongji University, 1239, Siping Rd., Shanghai, China

ARTICLE INFO

Article history:
Received 27 October 2016
Received in revised form 3 March 2017
Accepted 3 March 2017
Available online 6 March 2017

Keywords:
Evidence theory
Fatigue crack growth
Epistemic uncertainty
Uncertainty quantification
Differential evolution

ABSTRACT

Uncertainties originate from physical variability, data uncertainty, and modeling errors in the fatigue crack growth prediction analysis. This study presents an evidential uncertainty quantification (UQ) approach for determining uncertainties involved in revealing the material constants of the metal fatigue crack growth model with imprecise uncertainty information (i.e., epistemic uncertainty). The parameters in fatigue crack growth model are obtained by fitting the available sparse experimental data, and then the uncertainties in these parameters are considered. To alleviate the computational difficulties in the UQ analysis based on evidence theory, an interval optimization method based on differential evolution is used in finding the propagated belief structure. The overall procedure is demonstrated using the results of several replicated experiments on aluminum alloy CCT specimens.

1. Introduction

Uncertainties are prevalent in practical engineering applications and can be categorized as either aleatory uncertainty (also called objective, stochastic, and irreducible uncertainty) due to inherent variability in a physical phenomenon or epistemic uncertainty (also called subjective reducible uncertainty) due to unknown physical phenomena [1]. In the process of fatigue crack growth analysis, the various sources of uncertainty mainly include variability in loading conditions, material parameters, experimental data, and model uncertainty. These uncertainties can affect the analysis for fatigue crack propagation. Numerous experimental studies demonstrated that significant variability in crack propagation occurs even after crack initiation [2,3]. Uncertainty appears at different stages of analysis, and the interaction between these sources of uncertainty cannot be modeled easily. Thus, predicting fatigue behavior due to the various sources of uncertainty is difficult for design engineers or structural analysts.

Numerous uncertain models of crack propagation have been developed to deal with uncertainties observed in large replicate crack propagation tests and thus investigate the uncertainty of crack growth prediction. The quantification for the aleatoric uncertainties is relatively straightforward. Among the existing quantification techniques, Monte Carlo (MC) method is the most frequently used because of its moments than can represent a probability distribution. Karhunen–Loève [4] and polynomial chaos expansions [5] also have the same function. Besterfield et al. [6] combined probabilistic finite element analysis with reliability analysis to predict crack growth in plates. Liu and Mahadevan [7] proposed a concept of equivalent initial flaw size and used MC simulation to predict the probabilistic fatigue life. Jallouf et al. [8] employed probabilistic theory to investigate the reliability of undercut defect in a laser-welded plate made of Ti-6Al-4V titanium alloy. Blacha and Karolczuk [9] validated the effectiveness of the probabilistic model based on the weakest link concept in predicting the fatigue life of steel-welded joints. Fatigue and crack propagation in metals are recognized as stochastic processes [2,3]. Sarkar et al. [10] applied Wiener chaos expansions in estimating fatigue damage in randomly vibrating structures. Beck and Gomes [11] applied polynomial chaos in representing random crack propagation data, in which crack propagation in metals is recognized as a stochastic process. Riahi et al. [12] presented a stochastic collocation method for predicting random crack growth. Zhao et al. [13] combined stochastic collocation approach with Bayesian method in fatigue crack prognosis of metallic material, in which the distributions of random parameters are provided with certain types of distribution, such as normal distribution. Compared with the MC method, this approach is significantly more efficient and time saving and presents more accurate predictions. However, when sufficient data are unavailable or knowledge is lacking, the classical

* Corresponding author.
E-mail addresses: thstj@tongji.edu.cn (H. Tang), lidaweicc123@163.com (D. Li), 772551736@qq.com (J. Li), xue@tongji.edu.cn (S. Xue).

http://dx.doi.org/10.1016/j.ijfatigue.2017.03.004
0142-1123/

probability methodology may be inappropriate. Thus, strong statistical information cannot handle uncertainties in a fatigue lifetime prediction problem. In such a case, the usual probabilistic methodologies cannot be used and an alternative approach that can utilize insufficient uncertainty information is required.

Given experimental bounds on the variability of the Paris equation parameters, Worden and Manson [14] investigated the effect of the parameter uncertainty on the estimated lifetime of a cracked metallic plate (Titanium alloy Ti-6Al-4V) using interval arithmetic. Surace and Worden [15] conducted an extended analysis on damage progression within the framework of interval arithmetic. The major problem of the interval approach is that all ranges are entirely independent of one another and the upper and lower bounds are certain. This condition may result in the undesirable overestimation of the true solution set.

In general, the sources of aleatory uncertainty are represented using a probabilistic framework when sufficient data are available. By contrast, epistemic uncertainty cannot be fully characterized by probabilistic approaches because inferring any statistical information may be difficult owing to the lack of knowledge, thereby leading to subjective probabilistic descriptions. Epistemic uncertainty can be represented using various methods, such as interval arithmetic [16], fuzzy sets [17], possibility theory [18,19], information gap decision theory [20], evidence theory [21–24], and imprecise probability [25,26]. Selecting an appropriate mathematical structure to represent epistemic uncertainties can be more challenging than quantifying aleatory uncertainty. For example, the major difficulties in fuzzy set theory lie in that it cannot combine fuzzy sets with probabilistic information and cannot quantify the linguistic uncertainty. The possibility theory has no clear method for combining degrees of belief and probabilistic information. Among these methods, evidence theory has much potential in uncertainty quantification (UQ) and is more general than probability and possibility theories. Evidence theory was first proposed by Dempster [27] and extended by Shafer [21], which offers a framework for naturally modeling epistemic uncertainty and aleatory uncertainty due to its flexibility. It uses plausibility and belief to measure the likelihood of event without the need of additional assumptions. Evidence theory can provide equivalent formulations to convex models, possibility theory, and fuzzy sets, and it can incorporate different types of information in one framework to quantify uncertainty in a system [22]. Recently, some engineering applications with UQ based on evidence theory have achieved significant results [28–33].

Evidence theory has a strong capability to deal with uncertainty modeling and decision under uncertainty when the uncertainty information is imprecise. However, the large computational cost caused by its discrete property severely influences the practicability of evidence theory. To alleviate the computational difficulties in the UQ analysis based on evidence theory, an interval optimization based on differential evolution (DE) for computing bounds method is developed.

In this work, evidence theory is applied in characterizing the uncertainty of a fatigue crack growth model in situations where the uncertainty information is imprecise (i.e., epistemic uncertainty). The available data for the crack growth model material constants are insufficient for assigning a particular probability density function. In such a case, using only one framework (probability theory) to quantify the uncertainty in crack growth prediction may be limited. Thus, evidence theory that is notable for its flexibility and can offer a viable alternative for the purpose of uncertainty propagation is used. Fracture mechanics based on the Paris–Erdogan law [34] is chosen to describe the crack propagation, and initial crack size a_0 and the Paris equation constants C and m are regarded as uncertain variables. The fatigue crack growth data curve fitting analysis of the large replicate experimental results of Virkler et al. [2] and Tian et al. [35] is addressed. The present study aims to investigate the uncertainty of crack propagation using sparse experimental data to explore the feasibility of the approach.

2. Evidential UQ of crack growth model

2.1. Fundamentals of evidence theory

Evidence theory is introduced in this section prior to its application to the uncertainty modeling of crack growth. Evidence theory was originally proposed by Dempster [27] and further developed by Shafer [21] to describe epistemic uncertainty. Among the numerous non-probabilistic methods, evidence theory is the most closely related to probability theory, which is a generalization of classical probability theory. Probability masses can only be assigned to a single event in the UQ with probability theory, and the probability mass function is a mapping R: → [0, 1]. However, in evidence theory, the mass function is not only assigned to a single value but also to sets or ranges. The core of evidence theory is the frame of discernment Θ, which concludes all the possible answers to the investigated problem and all the elements in mutual exclusion between each other. Evidence theory is a mapping from $2^{\Theta} \rightarrow [0, 1]$. Mass function mapping is from $2^{\Theta} \rightarrow [0, 1]$, and A is a subset of 2^{Θ}, denoted by $A \subseteq 2^{\Theta}$. This mass function is given by

$$\begin{cases} m(\varnothing) = 0 \\ \sum\limits_{A \subseteq 2^{\Theta}} m(A) = 1 \end{cases}, \tag{1}$$

where $m(A)$ is also called basic belief assignment (BBA), and it represents confident degree in event A. When $m(A) > 0$, the subset A is called focal element. BBA is estimated by the obtained data or given by experience.

Evidence theory represents uncertainty using a probability interval instead of a probability value. For event A, the lower and upper bounds of uncertainty interval are called the belief function $Bel(A)$ and the plausibility function $Pl(A)$, respectively. $Bel(A)$ represents the confident degree to believe that event A is true, which is the minimum possibility that A occurs, and $Pl(A)$ represents the confident degree to believe that event A is not false, which is the maximum possibility that A occurs. $Bel(A)$ and $Pl(A)$ are given by

$$Bel(A) = \sum_{B \subseteq A} m(B), \tag{2}$$

$$Pl(A) = 1 - Bel(\bar{A}) = \sum_{B \cap A \neq \varnothing} m(B). \tag{3}$$

Belief and plausibility functions constitute the lower and upper bounds of proposition A. The interval $[Bel(A), Pl(A)]$ represents the belief degree of proposition A. For information from multiple sources, the combined evidence can be obtained by Dempster's rule [27] of combination. This rule is discussed in detail in [36].

2.2. Evidence-based UQ framework for fatigue crack growth models

Following the brief overview of evidence theory, the evidence-based UQ framework for fatigue crack growth models is presented in this section.

2.2.1. Crack propagation models

The proposed uncertain model of fatigue crack damage is based on a deterministic model of fatigue crack growth [34], which is based on the principle of linear elastic fracture mechanics. The Paris law provides the rate of crack propagation (da/dN) as a function of the amplitude of stress intensity factor (SIF) ΔK:

$$da/dN = C(\Delta K)^m \tag{4}$$

where C and m are the damage growth parameters. The parameters can vary by specimen because they greatly depend on the microstructure of material, and the effect of variability is the main focus of the study. The calculation of these unknown constants for a specific material requires fitting the crack growth model to experimental data. The SIF range for a center-cracked panel (the width of the crack is denoted by $2a$ and the width of the plate by $2w$) is calculated using Eq. (4). In Eq. (4), the SIF range ΔK in the given situation is generated simply because a time-varying stress $\sigma(t)$ can present a corresponding stress range $\Delta\sigma$.

$$\Delta K = \mathrm{Y}(\bar{a}) \cdot \Delta\sigma\sqrt{\pi a}, \tag{5}$$

where $\bar{a} = a/(2w)$ is a dimensionless parameter, $Y(\bar{a})$ is the parameter related to the size of geometry, and the analytical solution is $Y(\bar{a}) = 1$ for an infinite plate. Other several forms of $Y(\bar{a})$ for finite plate can be found in [14]. The UQ of the fatigue crack growth is essential to obtain the uncertainty of fatigue crack prediction lifetime (N) when uncertain parameters are provided. For a given crack growth model based on the framework with evidence theory, three major steps are involved in the UQ analysis. These steps are uncertainty representation, propagation, and measurement. The three steps are briefly described in the subsequent sections.

2.2.2. Uncertainty representation

For uncertainty representation, the UQ framework with evidence theory utilizes all possible obtained values of material constants provided by the experimental data to express the uncertain variables in interval form with assigned degree of belief. In this work, a general methodology described previously by Salehghaffari et al. [32] is adopted to obtain necessary information from available data and express the uncertain variables in the mathematical framework with evidence theory. The methodology is a two-step procedure, which involves representing uncertain parameters in interval form using all available data through generating a histogram for each model parameter and determining a suitable belief structure with assigned degree of belief for each parameter from the generated histogram depending on the relationship in the context of evidence theory. In this methodology, two adjacent intervals can be identified as having ignorance, agreement, or conflict relationship (Fig. 1). In Fig. 1, A and B are the number of data in adjacent intervals I_1 and I_2, respectively. The BBA for the three relationships is shown in Table 1. Ref. [32] provided the details on representation of uncertain parameters in intervals with assigned BBA.

Following the said two steps, the belief structure for single uncertain input is established. The evidential uncertainty representation is constructed by repeating the two steps for each uncertain parameter.

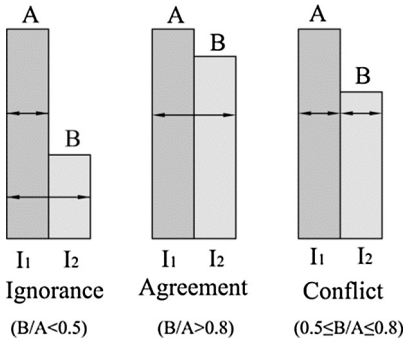

Fig. 1. Three relationships between adjacent intervals.

Table 1
BBA under three relationships.

Assignment of BBA	Ignorance $B/A < 0.5$	Agreement $B/A > 0.8$	Conflict $0.5 \le B/A \le 0.8$
$m(\{I_1\})$	$A/(A+B)$	Two adjacent intervals can be combined into one	$A/(A+B)$
$m(\{I_2\})$	0		$B/(A+B)$
$m(\{I_1, I_2\})$	$B/(A+B)$		0

2.2.3. Uncertainty propagation of fatigue life analysis

In the evidence theory community, uncertainty variable is usually expressed as a series of discrete focal elements based on limited information. Then, the uncertainty propagation is required to determine the belief structure of system response of interest that is influenced by the underlying material model uncertainties. Therefore, uncertainty propagation is a process of finding the maximum and minimum of the system response value in each hypercube interval (proposition of the joint belief structure). In propagating the represented uncertainties of crack growth model constants, final fatigue crack prediction lifetime N is considered the system response.

Considering the epistemic uncertainty of the system, the belief and plausibility functions of the response are obtained on the basis of the combined BBAs of the input parameters from different information sources using the evidence combination rules. The fatigue crack prediction response process $N = f(Y)$ has input parameter vector $\boldsymbol{Y} = (Y_1, \ldots, Y_n)$ with n variables of epistemic uncertainty. The joint proposition C of elementary proposition is constructed for the fatigue crack prediction system model as

$$C = \{\boldsymbol{c}_k = [x_{1i_1}, x_{2i_2}, \ldots, x_{ni_n}] : x_{1i_1} \in \boldsymbol{X}_1, x_{2i_2} \in \boldsymbol{X}_2, \ldots, x_{ni_n} \in \boldsymbol{X}_n\}, \tag{6}$$

where $\boldsymbol{X}_1, \boldsymbol{X}_2, \ldots, \boldsymbol{X}_n$ denote the interval sets of the n variables $Y_1, Y_2, \ldots, Y_n$. The relevant numbers of the intervals are $\boldsymbol{I}_1, \boldsymbol{I}_2, \ldots, \boldsymbol{I}_n$. $x_{1i_1}, x_{2i_2}, \ldots, x_{ni_n}$, $(i_1 \in [1, \boldsymbol{I}_1], i_2 \in [1, \boldsymbol{I}_2], \ldots, i_n \in [1, \boldsymbol{I}_n])$ denote the subintervals of $\boldsymbol{X}_1, \boldsymbol{X}_2, \ldots, \boldsymbol{X}_n$; c_k, $k \in [1, \boldsymbol{I}_1 \times \boldsymbol{I}_2 \times, \ldots, \times \boldsymbol{I}_n]$ denotes the n-dimensional joint proposition set constructed by several subintervals. The BBA of the joint proposition set C is defined as

$$m_c(\boldsymbol{c}_k) = m_1(x_{1i_1}) m_2(x_{2i_2}) \cdots m_n(x_{ni_n}). \tag{7}$$

Thus, every element of the Cartesian set C is required to be checked in the evaluation of the belief and plausibility functions by finding the system response bounds. In other words, the minimum and maximum responses of each joint set should be calculated as

$$[N_{\min}, N_{\max}] = [\min[f(\boldsymbol{c}_k)], max[f(\boldsymbol{c}_k)]]. \tag{8}$$

Given that uncertain variable is represented by many discontinuous sets instead of smooth and continuous explicit functions, the UQ with evidence theory becomes time consuming. Sampling and optimization are the two main approaches for finding the bounds of the system response. The accuracy of sampling approach is highly dependent on the number of samples and the number of hypercubes, and the process is extremely costly. On the contrary, optimization methods can dramatically reduce the computational work. To alleviate the said computational burden, the optimization approach in [37] based on DE [38] is used to calculate the response bounds of each hypercube and to compute the composite BBA of each hypercube, propagation of the represented uncertainty through fatigue crack growth model Eq. (4). The DE method is appropriate for such an interval bound task because of its derivative-free characteristics and discrete belief structure handling capability.

DE is a powerful stochastic real-parameter optimization algorithm for solving complex computational optimization problems.

As a novel evolutionary computation technique, DE resembles the structure of an evolutionary algorithm (EA). However, unlike traditional EAs, the DE variants perturb the current generation population members with the scaled differences of randomly selected and distinct population members. DE is a fast and robust algorithm that can be used as an alternative to EA because of the inherent characteristics of the former and other factors. Since the late 1990s, DE started to find several significant applications to the optimization problems arising from diverse domains of science and engineering. In a recently published article, Das and Suganthan [39] provided a comprehensive survey of the DE algorithm, including its basic concepts, different structures, and variants for solving various optimization problems as well as applications of the DE variants to practical optimization problems.

In the DE context, the individual trial solutions (constituting a population) are called parameter vectors or genomes. $S \in R^n$ is the search space of the problem. Then, the n-dimensional vector can be represented by $\boldsymbol{x}_i = (x_{i1}, x_{i2}, \ldots, x_{in})^T \in S$, $i = 1, 2, \ldots,$ NP. DE algorithm utilizes NP as a population for each iteration, called a generation of the algorithm. For the fatigue crack prediction response process, its parameter vector is generated by the uncertainty variables (a_0, C, and m) in ranges according to their respective belief structures. DE operates through the same computational steps as employed by a standard EA, including crossover, mutation, and selection operators. However, unlike traditional EAs, DE employs the difference in parameter vectors to explore the objective function landscape. The pseudo-code of DE is presented in Fig. 2. The detailed survey of the DE family of algorithms can be found in [38,39].

The DE-based computational strategy with the pseudo code of DE for finding the propagated belief structure is illustrated in Fig. 3 (only one uncertain parameter is considered). The procedure of uncertainty propagation using the DE strategy is as follows:

- For each uncertain parameter, collect all possible evidence, construct the BBA structure, and combine the BBA structures under the situation of pieces of evidence provided by different sources or experts using combination rules of evidence.
- Determine the joint BBA structure for multiple uncertain parameters by the Cartesian product operation.
- Use the DE algorithm to calculate the bound values of the system response within each joint interval and then construct the corresponding belief structures.
- Given the complete BBA on the output response of interest N, develop the belief and plausibility functions on N given any general subset by applying Eqs. (4) and (5).

2.2.4. Uncertainty measurement

After obtaining the BBA structure of the crack growth model response, observed evidence on simulation responses is used in determining the target propositions to estimate uncertainty measures, namely, *Bel* and *Pl*. Given the propagated focal elements and associated belief structure as $([N_{1,\min}, N_{1,\max}], m_1), \ldots, ([N_{i,\min}, N_{i,\max}], m_i), \ldots, ([N_{n,\min}, N_{n,\max}], m_n)$, the evidential measures of target proposition $A = [N_{A,\min}, N_{A,\max}]$ can be written as

$$Bel(A) = \sum_{[N_{i,\min}, N_{i,\max}] \subseteq [N_{A,\min}, N_{A,\max}]} m_i, \tag{9}$$

$$Pl(A) = \sum_{[N_{i,\min}, N_{i,\max}] \cap [N_{A,\min}, N_{A,\max}] \neq \varnothing} m_i. \tag{10}$$

In practical implementation of risk analysis and reliability study, the probability bounds are preferred than the uncertainty measures on single target proposition. Ferson et al. [40] constructed the cumulative belief function (CBF), which is also indicated as the right probability bound of p-box, and the cumulative

Step1: Set the values of mutation constants F, crossover constants CR, population size NP, maximum numbers of generations G_{max}, object function $f()$, and number of parameters of object function ID

Step 2: Randomly initialize the NP population $\boldsymbol{x}_i^0$ (i<=NP) and select the best competitor $\boldsymbol{x}_{best}^0$

Step3: WHILE G<=G_{max} or convergence criterion is not satisfied

FOR i=1 to NP

***3.1 Mutation step*:** the mutated vector is generated as

$$v_i^{G+1} = x_i^G + F_1\left(x_{best}^G - x_i^G\right) + F\left(x_{r1}^G - x_{r2}^G\right)$$

***3.2 Cross step*:** for each mutated vector, the trial vector is generated using

FOR j=1 to ID

IF rand(j)≤CR or j=randn(i) THEN $u_{ij}^{G+1} = v_{ij}^{G+1}$

OTHERWISE $u_{ij}^{G+1} = x_{ij}^{G+1}$

END IF

END FOR

3.3 Selection step: Evaluate each trial vector $u_i^{(G+1)}$

IF $f(u_i^{G+1}) < f\left(x_i^{G+1}\right)$ THEN $x_i^{G+1} = u_i^{G+1}$

OTHERWISE $x_i^{G+1} = x_i^G$

IF $f(x_i^{G+1}) < f\left(x_{best}^G\right)$ THEN $x_{best}^{G+1} = x_i^{G+1}$

OTHERWISE $x_{best}^{G+1} = x_{best}^G$

END IF

END IF

END FOR

3.4 Increment the generation count G=G+1

END WHILE

Fig. 2. DE pseudo code.

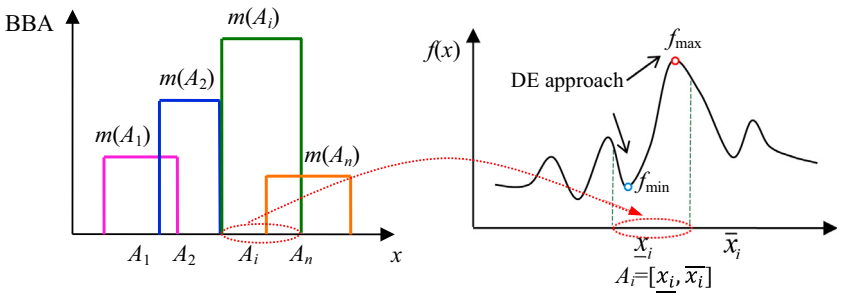

Fig. 3. Finding system propagated belief structure by DE.

plausibility function (CPF), which is also indicated as the left probability bound of p-box. Given the propagated focal elements and associated belief structure $([N_{1,\min}, N_{1,\max}], m_1), \ldots, ([N_{i,\min}, N_{i,\max}], m_i), \ldots, ([N_{n,\min}, N_{n,\max}], m_n)$, the lower and upper probability bounds of the threshold value of fatigue life N_{thre} can be obtained as

$$\underline{P}(N_{\text{thre}}) = \sum_{N_{i,\max} \leqslant N_{\text{thre}}} m_i, \tag{11}$$

$$\overline{P}(N_{\text{thre}}) = \sum_{N_{i,\min} \leqslant N_{\text{thre}}} m_i. \tag{12}$$

The UQ framework of evidence theory using DE optimization is shown in Fig. 4.

3. Numerical and experimental studies

3.1. Tian et al.'s [35] data set

The uncertainty of fatigue crack growth prediction is investigated using experimental data of 2024-T42 aluminum alloy specimens (Fig. 5) under constant-amplitude loading ($P_{\max}$ = 25.0 kN, $P_{\min}$ = 12.5 kN) given by Tian et al. [35]. The geometrical dimensions of the plate and load are as follows: width of 100 mm, thickness of 4 mm, stress range $\triangle\sigma$ = 32.5 MPa (i.e., $\sigma_{\max}$ = 65 MPa corresponding to the maximum applied load of 25.0 kN), and the load ratio R of 0.5. A total of 14 sets of 2024-T42 aluminum alloy specimen experiments are conducted in [35], and the corresponding experimental data are listed in Tables 2–4.

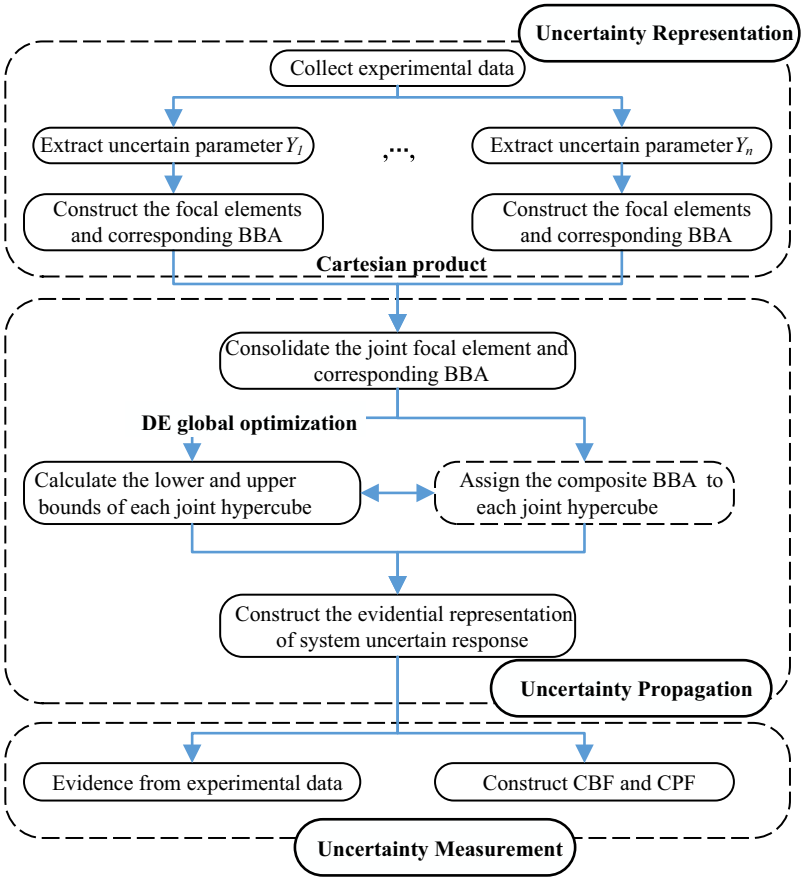

Fig. 4. Procedure of UQ using DE global optimization method for crack growth analysis.

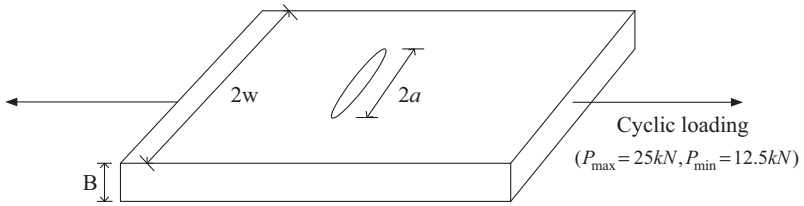

Fig. 5. Thin rectangular plate under uniaxial tension.

Table 2
Test data of fatigue crack growth length of 2024-T42 aluminum alloy (mm).

N	*i*													
	1	2	3	4	5	6	7	8	9	10	11	12	13	14
0	5.55	5.40	5.30	5.20	5.25	5.30	5.25	5.40	5.30	5.25	5.40	5.30	5.40	5.25
5000	6.15	5.80	5.70	5.50	5.75	5.40	5.55	5.83	5.80	5.60	5.90	5.60	5.75	5.63
10,000	6.75	6.30	6.30	6.08	6.45	5.75	6.05	6.35	6.28	6.10	6.30	6.05	6.35	6.20
15,000	7.50	6.90	6.90	6.55	7.20	6.20	6.55	6.95	6.90	6.70	6.75	6.55	7.15	6.80
20,000	8.25	7.50	7.70	7.10	8.00	6.75	7.25	7.65	7.55	7.25	7.60	7.25	7.90	7.50
25,000	9.25	8.25	8.50	7.65	8.85	7.30	8.00	8.45	8.40	8.10	8.35	7.85	8.65	8.38
30,000	10.25	9.10	9.45	8.25	10.00	8.00	8.90	9.25	9.15	9.00	9.15	8.60	9.75	9.30
35,000	11.25	10.00	10.55	9.05	11.20	8.75	9.80	10.25	10.15	9.90	10.15	9.35	10.90	10.25
40,000	12.65	11.10	11.60	9.85	12.60	9.55	11.00	11.20	11.10	11.35	11.25	10.35	12.25	11.40
45,000	14.50	12.60	13.00	10.75	14.90	10.45	12.40	12.50	12.35	12.80	12.75	11.50	13.90	12.75
50,000	17.25	14.45	14.70	11.75	17.95	11.75	14.10	14.25	14.15	14.75	14.65	13.00	16.60	14.95
52,500	19.80								14.90	16.05	15.60	13.85	17.75	16.25
55,000	21.85	15.55	15.90	12.30	20.00		15.05	15.05	16.10	17.60	17.00	15.00	21.75	17.90
57,500	26.05	16.90	17.60	13.20		13.65	16.35	16.30	17.50	19.50	18.75	16.75	26.25	20.25
60,000		18.55	19.35	14.25	24.00		17.90	17.75	19.45	23.00	20.60	18.50		23.90
58,000	27.25	20.35	21.75	15.60		16.30	20.00	19.75						
58,500	29.25													
59,000	31.70													
61,000			22.65	17.10			21.00	20.55	20.20	25.50		19.45		25.90
62,000		22.50	23.75			20.00	22.25	21.50	21.00	27.35		20.45		29.90
63,000			25.30	18.75			24.25	22.75	22.30			21.50		
64,000		25.00	28.75	19.			26.60	24.25	23.75			22.55		
65,000		27.70		75			30.10	25.50	27.10			24.00		
66,000		30.10		20.95								26.25		
67,000				22.25										
68,000				24.15		22.85								
69,000				26.50										
70,000				30.25		25.80								

Table 3
Initial and critical crack length for every specimen (mean value of left and right length).

No.	1	2	3	4	5	6	7	8	9	10	11	12	13	14
Initial size(mm)	5.50	5.40	5.30	5.20	5.25	5.30	5.25	5.40	5.30	5.25	5.40	5.30	5.40	5.25
Critical size(mm)	32.5	31.5	33.0	32.0	31.0	32.0	33.0	32.5	32.0	32.0	32.0	32.0	32.0	32.5

Table 4
Fatigue crack growth lifetime (number of cycles) for every specimen.

No.	1	2	3	4	5	6	7	8	9	10	11	12	13	14
N	59,045	66,146	64,489	70,192	57,103	71,404	65,494	66,811	67,678	62,871	66,141	66,935	58,844	62,370

For the uncertainty representation of material constants using evidence theory, separate belief structures for each uncertain parameter (three material constants of growth rates equation) should be constructed. The derived data for material constants of fatigue crack growth model (Tables 3 and 4) reflect the uncertainty in behavior of the 2024-T42 aluminum alloy and is thus used as available evidence in the construction of belief structures.

In general, the Paris law can be conveniently written in the logarithm form as

$$\lg(da/dN) = \lg C + m\lg(\Delta K). \tag{13}$$

The material constants of 2024-T42 aluminum alloy are determined using the experimental data provided in [35]. Least squares curve fitting the growth rates in Eq. (13) with Bicoudate function using a_i-N_i data in Table 2 yields the corresponding Paris parameters C and m, as shown in Table 5. The average relative fitting deviations of crack length and crack growth ratio are also listed in Table 5.

In accordance with Salehghaffari et al.'s [32] criterion, the data distribution and the corresponding belief structure for uncertain material constants C, m, and a_0 are constructed for 2024-T42 aluminum alloy using the data provided in Tables 3 and 5, as shown in Fig. 6(a)–(c).

Table 5
Fitting results of parameters C and m.

No.	Material constants C ($\times 10^{-10}$)	m	Relative deviation (%)	No.	Material constants C ($\times 10^{-10}$)	m	Relative deviation (%)
1	5.58	3.49	2.57	8	9.25	3.14	1.97
2	7.33	3.28	2.87	9	6.28	3.37	5.02
3	8.69	3.21	4.31	10	6	3.44	2.89
4	2.86	3.81	3.10	11	10.64	3.06	2.00
5	11.45	3.12	2.03	12	4.73	3.53	1.68
6	3.18	3.70	6.87	13	6.74	3.38	3.63
7	4.72	3.55	1.87	14	5.23	3.52	2.51

For the first case study, the Paris parameters are taken from the experimental data in Table 5 with assumption of independence. The fatigue crack propagation lifetime can be obtained through numerical integration of Eq. (4). The average value of critical size $a_c = 32$ mm in Table 3 is used to denote the failure criteria of specimen. Therefore, the subsequent calculations are all terminated when $a = a_c$, and failure is then assumed to occur immediately. Using the belief structures of C, m, and a_0 listed in Fig. 6, the lower and upper bounds of each joint focal element are obtained by the framework of uncertainty propagation. For comparison with probability theory, the logarithmic normal distribution is used to model C [41], the normal distribution is used to model m [41], and the uniform distribution is used to model the initial size of crack a_0. The distribution information are listed in Table 6.

Employing the uncertain information in Table 6, MC sampling is performed 10,000 times in the variable interval $[u \pm 3\sigma]$, and the CDF curve of fatigue life N is shown in Fig. 7. Using Eqs. (11) and (12), the CBF and CPF of fatigue life are obtained as shown in Fig. 7. To investigate the characters of UQ of probability theory, evidence theory, and the interval analysis, the interval-based uncertainty representation and propagation for $C = [1.06, 9.25] \times 10^{-10}$, $m = [3.06, 3.81]$, and $a_0 = [5.2, 5.5]$ are also performed. The corresponding lower and upper bounds of interval calculation are shown in Fig. 7. As the representative value, the left and right probability bounds for the expectation of experimental fatigue life $\overline{N} = 64,680$ are presented in Fig. 7. The estimated belief and plausibility of 95% confidence intervals for fatigue lifetime are also listed in Fig. 7.

In comparison with the fatigue life interval of experimental data $N = [57,103, 71,404]$, the prediction values of the three prediction methods are distributed in a huge range for the estimated lifetime as presented in Fig. 7. For the expectation of experimental fatigue life $\overline{N}$, the probability is 0.502 and the interval calculation is [0, 1]. Using Eqs. (11) and (12), the right and left probability bounds of $\overline{N} = [0.209, 0.755]$ are presented by evidence theory. Meanwhile, probability theory and evidence theory overestimate (i.e., 25,954 and [21,062, 41,809]) the actual solution set with 95% guarantee probability. The estimates of the lifetime cannot be used as the

Table 6
Distribution information of C, m, and a_0.

Uncertain parameter	Distribution type	Distribution parameters	
C	Logarithmic normal	$\ln u = -22.22$	$\sigma = 0.576$
m	Normal	$u = 4.073$	$\sigma = 0.331$
a_0	Uniform	[5.20, 5.50]	

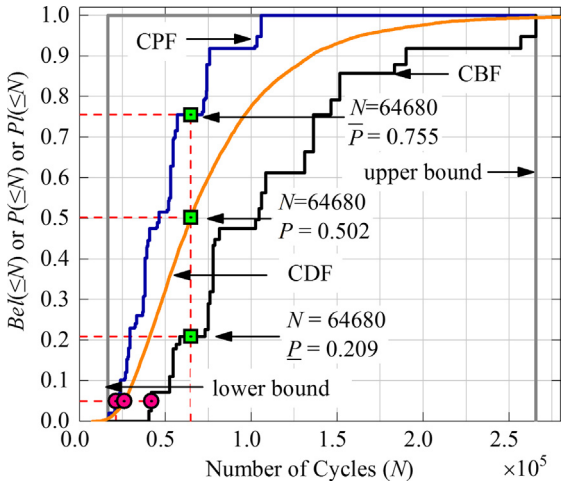

Fig. 7. Fatigue lifetime cumulative distributions of evidence theory and probability theory with parametric independence.

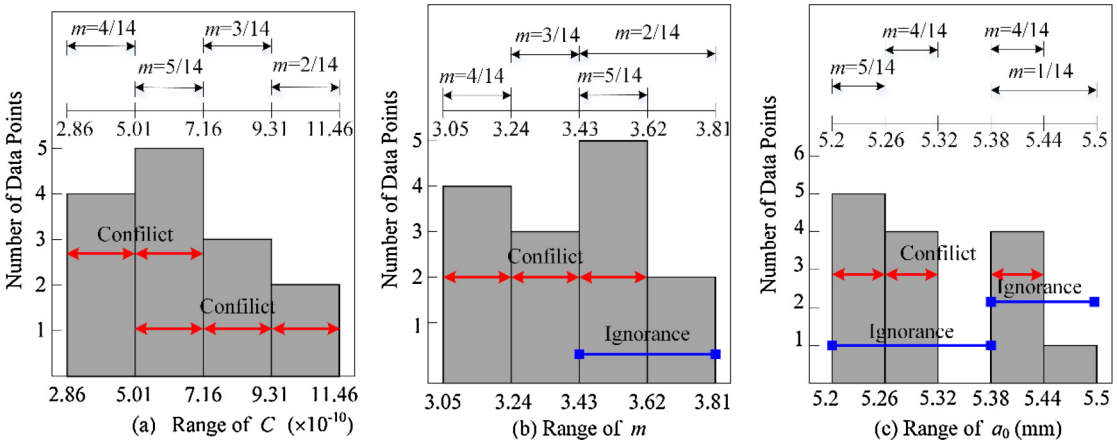

Fig. 6. Data distribution and corresponding belief structure of parameters C, m, and a_0.

lower and upper bounds in each case because of the parametric independence.

The uncertainty measures (*Bel* and *Pl*) are used to access the belief degree of a defined target proposition set using the propagated belief structure. The nominal value $\overline{N} = 64,680$ and standard derivation $\sigma = 4216$ of the experimental data are employed to define the three target propositions with different level scatters as follows: $[0.975\overline{N}, 1.025\overline{N}]$. $[0.95\overline{N}, 1.05\overline{N}]$, and $[\overline{N}-\sigma, \overline{N}+\sigma]$. According to Eqs. (9) and (10), the value of *Bel* and *Pl* can be estimated by adding the BBA of propagated focal elements that fall into the target proposition and that intersect with target proposition, respectively. The value of three target propositions is presented in Table 7.

Table 7 shows that the change in the uncertain measures (*Bel* and *Pl*) of different target propositions is inconsistent with the interval extension of the target proposition. Although the range of target proposition varies from [63,063, 66,297] to [60,465, 68,896], the value of *Bel* and *Pl* are fixed at 0 and 0.5459, respectively. As shown in Fig. 7 and Table 7, the overestimation of fatigue life is attributed to the lack of experimental data and interval explosion of ignoring the dependence of C and m. The resulting interval range can be effectively reduced by considering the dependencies between the parameters to reduce the effect of the parametric uncertainty on the estimated lifetime. In the subsequent analysis, Paris parameters are assumed to be statistically dependent, and the least square method is used to estimate the statistical correlation from the data set. However, using the data set as the 14 samples in the tests may be inappropriate.

Despite the uncertain views on the derivation, the relationship between C and m as fully described by $\lg C = \alpha + \beta m$ is acknowledged by many studies (e.g., [42–46]). Fig. 8 shows the fitting line of $\lg C$ and m with correlation coefficient $R = -0.988$. The critical correlation coefficient R_0 is 0.66 when $n = 14$ and $R > R_0$. This condition indicates that $\lg C$ and m are significantly linearly correlated. Therefore, the correlation between the parameters should be considered in this fatigue lifetime estimation.

In accordance with the fitting result of $\lg C$ and m shown in Fig. 8, the nominal value $\lg C_{\text{nom}}$ of coefficient $\lg C$ is formulated as the linear expression of exponent m. Furthermore, the uncertainty of C can be expressed as C_{nom} and a residual error ε [47], and the belief structure of residual error ε is provided in Fig. 9.

$$C = (1+\varepsilon)C_{\text{nom}} \tag{14}$$

Introducing the uncertain information of uncertain parameters m and ε into the evidential UQ framework presented in Section 3 yields the uncertainty propagation results. Similar to the independence case, the uncertainty measures (*Bel* and *Pl*) are used to estimate the belief degree of target proposition under the condition of the correlation between C and m. Table 8 lists the value of *Bel* and *Pl* for the target proposition as follows: $[0.975\overline{N}, 1.025\overline{N}]$. $[0.95\overline{N}, 1.05\overline{N}]$, and $[\overline{N}-\sigma, \overline{N}+\sigma]$.

Table 8 shows that the evaluated values of *Bel* and *Pl* of experimental precision intervals of fatigue life obviously increase as the target proposition enlarges. Compared with the independence case, the range of *Bel* and *Pl* becomes much tighter. This tendency is due to the reduction in epistemic uncertainty of fatigue life

Table 7
Evidential measurement for experimental precision intervals of fatigue life.

Target proposition	Precision	Fatigue life (N)	
		Bel	*Pl*
[63,063, 66,297]	97.5%	0	0.5459
[61,446, 67,914]	95%	0	0.5459
[60,465, 68,896]	$\overline{N} \pm \sigma$	0	0.5459

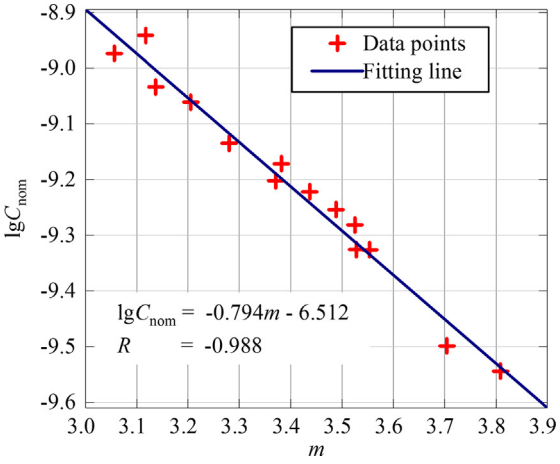

Fig. 8. Correlation between lg$C$ and m.

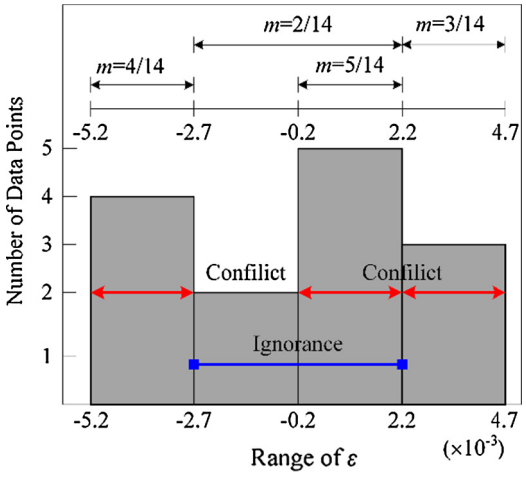

Fig. 9. Data distribution and belief structure of ε.

Table 8
Evidential measurement for experimental precision intervals of fatigue life.

Target proposition	Precision	Fatigue life (N)	
		Bel	*Pl*
[63,063, 66,297]	97.5%	0	0.5357
[61,446, 67,914]	95%	0.09	0.8955
[60,465, 68,896]	$\overline{N} \pm \sigma$	0.1678	1

N. Fig. 10 shows the estimated CBF, CPF, and CDF curves of the fatigue lifetime. The estimated belief and plausibility for 95% experimental precision intervals for fatigue lifetime, and some results of MC simulation and interval calculation are summarized in Table 9.

As shown in Fig. 10 and Table 9, the scope of the estimated lifetime for the three methods significantly decreases when considering the parametric dependency as expected. Given such consideration, the epistemic uncertainty in fatigue crack modeling significantly decreases. With an appropriate fatigue crack modeling, the estimated bounds enclose any experimentally measured data and actually yield usable estimates for the specimen lifetime. Therefore, despite the availability of experimentally obtained Paris law coefficients, considering the nature of parametric dependency should still be considered cautiously.

Evidence theory can effectively handle uncertain variables without exact probability distribution, and it excellently avoids

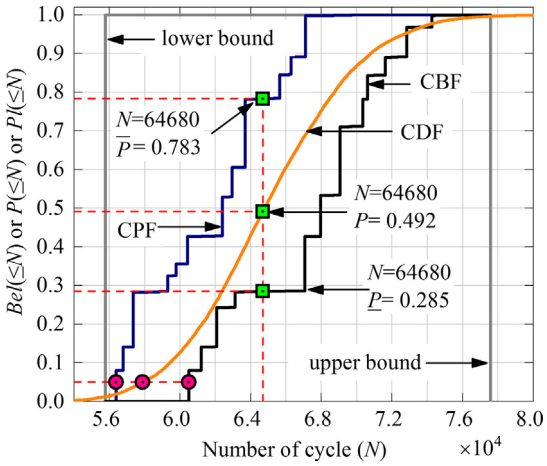

Fig. 10. Fatigue crack propagation lifetime cumulative distribution under parametric dependency.

Table 9
Calculation results of three methods under parametric dependency.

Results	Evidence theory	MC	Interval calculation
95%	[56,375, 60,493]	57,878	–
Entire range	[55,760, 77,576]	[51,784, 82,349]	[55,760, 77,576]

the error caused by probability theory. For example, the result calculated by probability theory shows that the probability is no more than 5% when the lifetime exceeds 57,878, while the result by evidence theory is [56,375, 60,493]. The conservative estimation of lifetime by evidence theory shows the minimum value of 56,375. In particular, evidence theory provides the prognosis for the assumed specimen as the interval [56,375, 60,493] with 95% guarantee probability, and estimated lifetime can be set as 56,375 to ensure the safety. Compared with the experimental results, the lifetime of 14 specimens is all larger than 56,375, and the maximum deviation is 26.7%. The gap between belief and plausibility for experimental precision intervals reflects the epistemic uncertainty embedded in the fatigue growth model.

3.2. Virkler et al.'s [2] data set

The impact of sparse experimental data (epistemic uncertainty) on fatigue crack lifetime prediction analysis is resolved using the large replicate experimental results of Virkler et al. [2]. The tests involve 2024-T3 aluminum sheets with a 9 mm pre-centered crack. These sheets are subjected to a cyclic loading with a maximum load of 23 kN and a stress ratio of $R = 0.2$, and the loading is terminated with the critical size $a_c = 49.8$ mm. Each of the 68 specimens tested is observed 163 times. Significant scatter can be observed in the resulting $\ln[da/dN]$ versus $\ln[\Delta K]$ data. Further details can be found in [2].

An imprecise information situation can be assumed due to the lack of information or data in the current example. In the example, two data sets (11 and 68 specimens) are randomly selected from the experimental results of 68 specimens. These data sets are then used to quantify uncertainty for the fatigue crack lifetime predictions. Considering the nature of parametric dependency, only parameter m in the fatigue crack growth model is obtained by fitting the available sparse experimental data (11 and 68 specimens). The correlation relationship is shown in Fig. 11. The data distribution and the corresponding belief structure of m and residual error ε using 11 specimens are shown in Fig. 12 (a) and (b), and those for 68 specimens are shown in Fig. 13.

The evidential propagation results are obtained using the belief structures of m and ε listed in Figs. 12 and 13. Similar to the first case study, three different-level target propositions $[0.975\overline{N}, 1.025\overline{N}]$, $[0.95\overline{N}, 1.05\overline{N}]$, and $[\overline{N}-\sigma, \overline{N}+\sigma]$ are used in this part to investigate the application of evidential measurement. The uncertainty measurement of the three target propositions using 11 and 68 specimens are presented in Tables 10 and 11, respectively.

Comparing the results presented in Tables 10 and 11 shows that the *Bel* and *Pl* of experimental precision intervals of fatigue life obviously increase as the target proposition enlarges. The range of the two measurements also becomes tighter. This condition is attributed to the accumulation of experimental data. For comparison with the probability theory, the uncertain parameter exponent m and residual error ε are estimated as normal distribution. The distribution parameters are listed in Table 12.

Using the uncertain information presented in Table 12, MC simulation is implemented 10,000 times in the variable interval $[u \pm 3\sigma]$, and the probabilistic results are shown in Fig. 14 (a) and (b). The CPF and CBF curves of the number of cycles using 11 and 68 specimens are also shown in Fig. 14. The left and right probability bounds for the expectation of experimental fatigue life $\overline{N} = 2.57 \times 10^5$ are presented in Fig. 14.

Fig. 14(b) shows that the right and left probability bounds are 0.588 and 0.847, respectively, for fatigue lifetime at the cycle number of $\overline{N} = 2.57 \times 10^5$. The results show that the fatigue lifetime probability is as high as 0.847 and as low as 0.588, and this condition can be written as a probability interval [0.588, 0.847]. Similarly, the probability intervals obtained at the given number of cycles by use of 11 specimens are represented as interval [0.438,

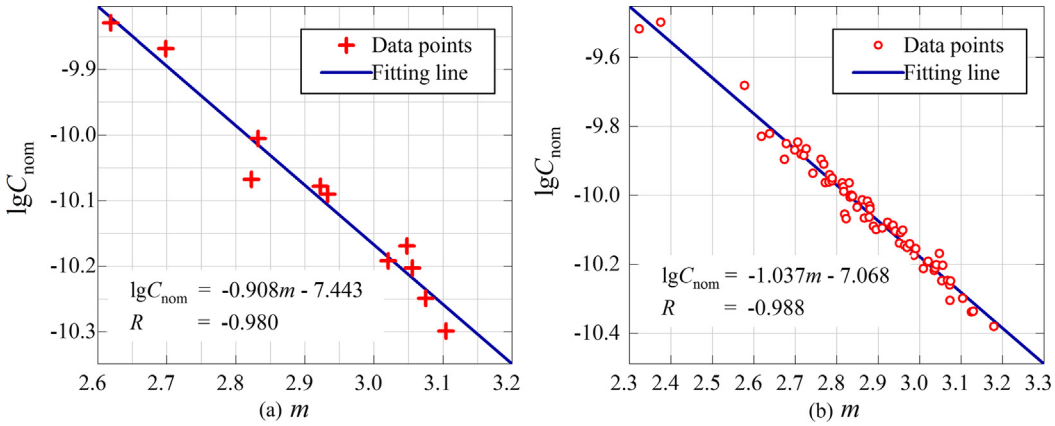

Fig. 11. Correlation between lg$C$ and m using (a) 11 and (b) 68 specimens.

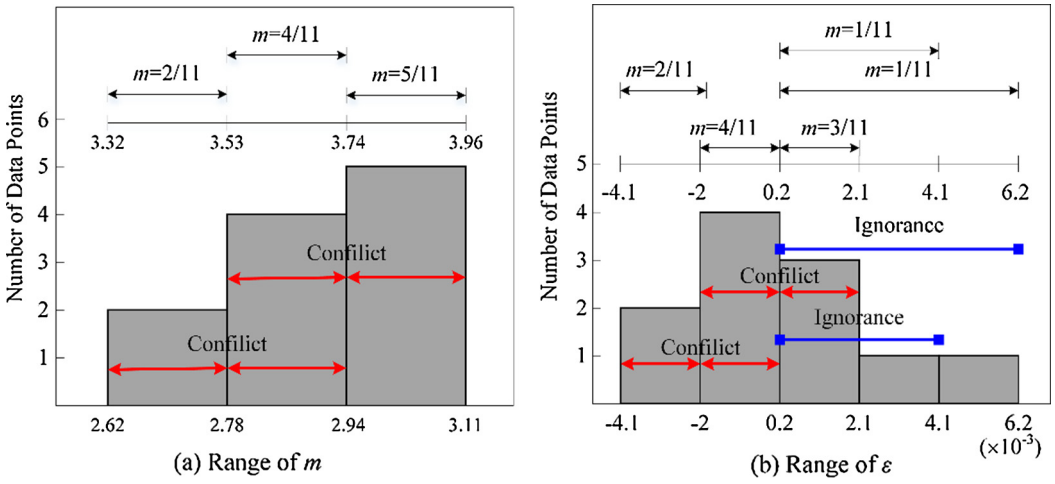

Fig. 12. Data distribution and corresponding belief structure of (a) m and (b) ε using 11 specimens.

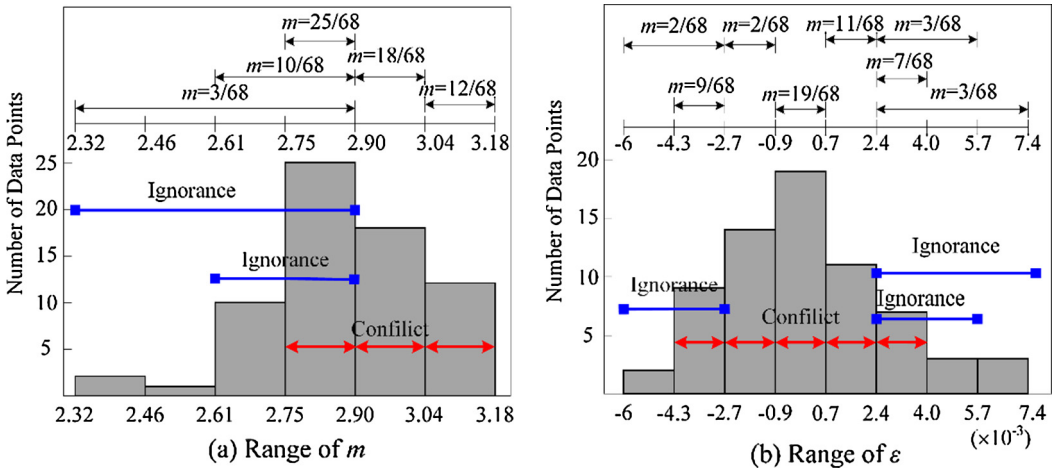

Fig. 13. Data distribution and the corresponding belief structure of (a) m and (b) ε using 68 specimens.

Table 10
Evidential measurement for experimental precision intervals of fatigue life using 11 specimens.

Target proposition	Precision	Fatigue life (N)	
		Bel	*Pl*
$[2.507, 2.636] \times 10^5$	97.5%	0	0.6860
$[2.443, 2.700] \times 10^5$	95%	0	0.7521
$[2.387, 2.756] \times 10^5$	$\overline{N} \pm \sigma$	0.1	0.9174

Table 11
Evidential measurement for experimental precision intervals of fatigue life using 68 specimens.

Target proposition	Precision	Fatigue life (N)	
		Bel	*Pl*
$[2.507, 2.636] \times 10^5$	97.5%	0	0.518
$[2.443, 2.700] \times 10^5$	95%	0.173	0.752
$[2.387, 2.756] \times 10^5$	$\overline{N} \pm \sigma$	0.396	0.833

0.917], as shown in Fig. 14(a). When the number of sample sizes increases, the bounds of evidence theory in Fig. 14(b) become much smaller in quantity compared with those in Fig. 14(a), and the "stair-step" of evidence theory appears smoother. Therefore, the bounds of number of cycle probability are accurate and adequate [48,49]. This deduction also shows that the three measurements (belief, probability, and plausibility) eventually converge to a single value with sufficiently increasing data information. The 95 guarantee left and right probability bounds of estimated intervals for fatigue lifetime are provided in Table 13. The results of MC simulation are also listed in Table 13.

Table 13 shows that the estimated intervals of evidence theory and MC simulation become close to experimental precision intervals when experimental data are highly available. In addition, the 95% precision intervals of evidence theory using 68 specimens are much smaller in quantity compared with those using 11 specimens. In summary, the accuracy in parametric UQ using evidence theory increases when sufficient data are available.

Table 12
Distribution information of m, and ε.

Sample size	Uncertain parameter	Distribution type	Distribution parameters	
11	m	Normal	$u = 2.921$	$\sigma = 0.161$
	ε	Normal	$u = 0$	$\sigma = 2.9 \times 10^{-3}$
68	m	Normal	$u = 2.874$	$\sigma = 0.165$
	ε	Normal	$u = 0$	$\sigma = 2.7 \times 10^{-3}$

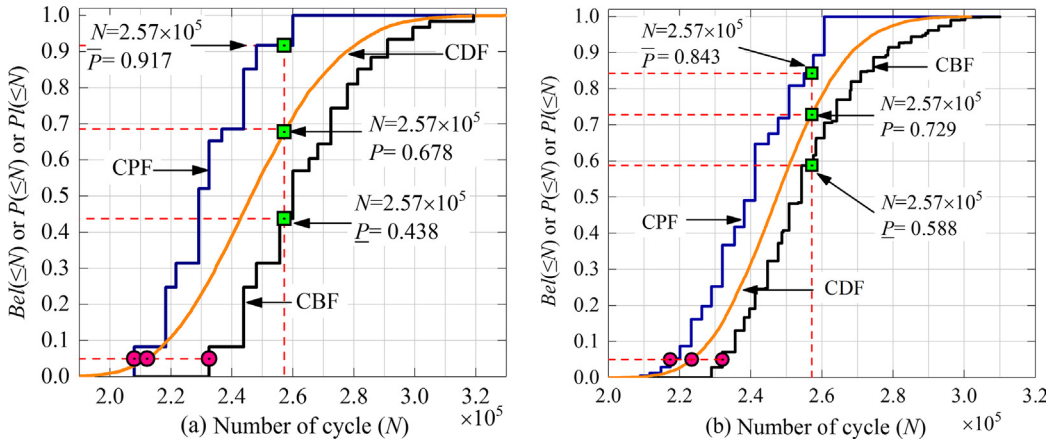

Fig. 14. Fatigue crack propagation lifetime cumulative distribution for (a) 11 and (b) 68 specimens.

Table 13
Estimated results of sparse experimental data.

Sample size	Results	Evidence theory	Monte Carlo	Test data
11	95%	$[2.080, 2.325] \times 10^5$	2.122×10^5	–
	Entire range	$[2.080, 3.193] \times 10^5$	$[1.776, 3.311] \times 10^5$	$[2.228, 3.210] \times 10^5$
68	95%	$[2.173, 2.320] \times 10^5$	2.234×10^5	–
	Entire range	$[2.088, 3.100] \times 10^5$	$[1.986, 3.018] \times 10^5$	$[2.228, 3.210] \times 10^5$

4. Conclusions

In this article, epistemic UQ of crack propagation data using evidence theory is presented. The evidential reasoning approach using differential evolution provides a computationally efficient framework for UQ of material constants in Paris crack growth model under epistemic uncertainty. Uncertainty analysis of large replicate experimental results (such as that of Virkler et al. [2] and Tian et al. [35]) verifies the presented approach for the Paris model and its potential applicability to other similar material models. Notwithstanding the high efficient of DE based evidential UQ framework, the computational burden is still the major challenge due to exponential increase of joint focal elements of complex and large scale problems. The advanced surrogated models are expected to cope with this scenario.

The epistemic uncertainty of the estimated lifetime is significantly decreased when considering the parametric dependency and the increase in the number of sample sizes as expected. The results of several replicated experiments show significant scatter of Paris damage model parameters. This condition implies that the existing deterministic analysis may be non-conservative, and the epistemic uncertainties in Paris damage model should be considered in fatigue crack lifetime prediction analysis.

Acknowledgments

This study was supported by the Ministry of Science and Technology of China (Grant No. SLDRCE14-B-03), National Natural Science Foundation of China (Grant No. 51178337), and Natural Science Foundation of Shanghai (Grant No. 17ZR1431900).

References

[1] Oberkampf WL, Helton JC, Sentz K. Mathematical representation of uncertainty. Am. Inst. Aeronaut. Astronaut. In: Non-deterministic approaches forum, Seattle, WA; 2001. p. 1–23. http://dx.doi.org/10.2514/6.2001-1645.
[2] Virkler DA, Hillberry B, Goel PK. The statistical nature of fatigue crack propagation. J Eng Mater Technol 1979;101:148–53. http://dx.doi.org/10.1115/1.3443666.
[3] Ghonem H, Dore S. Experimental study of the constant-probability crack growth curves under constant amplitude loading. Eng Fract Mech 1987;27:1–25. http://dx.doi.org/10.1016/0013-7944(87)90002-6.
[4] Mathar RJ. Karhunen-Loève basis of Kolmogorov phase screens covering a rectangular stripe. Waves Random Complex Media 2010;20:23–35. http://dx.doi.org/10.1080/17455030903369677.
[5] Xiu D. Numerical methods for stochastic computations: a spectral method approach. Princeton: Princeton University Press; 2010.
[6] Besterfield GH, Liu WK, Lawrence MA, Belytschko T. Fatigue crack growth reliability by probabilistic finite elements. Comput Methods Appl Mech Eng 1991;86:297–320. http://dx.doi.org/10.1016/0045-7825(91)90225-U.
[7] Liu Y, Mahadevan S. Probabilistic fatigue life prediction using an equivalent initial flaw size distribution. Int J Fatigue 2009;31:476–87. http://dx.doi.org/10.1016/j.ijfatigue.2008.06.005.
[8] Jallouf S, Casavola K, Pappalettere C, Pluvinage G. Assessment of undercut defect in a laser welded plate made of Ti–6Al–4V titanium alloy with probabilistic domain failure assessment diagram. Eng Fail Anal 2016;59:17–27. http://dx.doi.org/10.1016/j.engfailanal.2015.11.018.
[9] Blacha Ł, Karolczuk A. Validation of the weakest link approach and the proposed Weibull based probability distribution of failure for fatigue design of steel welded joints. Eng Fail Anal 2016;67:46–62. http://dx.doi.org/10.1016/j.engfailanal.2016.05.022.
[10] Sarkar S, Gupta S, Rychlik I. Wiener chaos expansions for estimating rain-flow fatigue damage in randomly vibrating structures with uncertain parameters. Probabilist Eng Mech 2011;26:387–98. http://dx.doi.org/10.1016/j.probengmech.2010.09.002.
[11] Beck AT, Santana GWJDe. Stochastic fracture mechanics using polynomial chaos. Probabilist Eng Mech 2013;34:26–39. http://dx.doi.org/10.1016/j.probengmech.2013.04.002.
[12] Riahi H, Bressolette P, Chateauneuf A. Random fatigue crack growth in mixed mode by stochastic collocation method. Eng Fract Mech 2010;77:3292–309. http://dx.doi.org/10.1016/j.engfracmech.2010.07.015.
[13] Zhao F, Tian Z, Zeng Y. A stochastic collocation approach for efficient integrated gear health prognosis. Mech Syst Signal Process 2013;39:372–87. http://dx.doi.org/10.1016/j.ymssp.2013.03.004.
[14] Worden K, Manson G. Prognosis under uncertainty – an idealised computational case study. Shock Vib 2008;15:231–43. http://dx.doi.org/10.1155/2008/958343.
[15] Surace C, Worden K. Extended analysis of a damage prognosis approach based on interval arithmetic. Strain 2011;47:544–54. http://dx.doi.org/10.1111/j.1475-1305.2011.00815.x.
[16] Muhanna RL, Mullen RL. Uncertainty in mechanics problems-interval-based approach. J Eng Mech 2001;127:557–66. http://dx.doi.org/10.1061/(ASCE)0733-9399(2001)127:6(557).
[17] Hanss M, Turrin S. A fuzzy-based approach to comprehensive modeling and analysis of systems with epistemic uncertainties. Struct Saf 2010;32:433–41. http://dx.doi.org/10.1016/j.strusafe.2010.06.003.
[18] Youn BD, Choi KK, Du L, Gorsich D. Integration of possibility-based optimization and robust design for epistemic uncertainty. J Mech Des 2007;129:876–82. http://dx.doi.org/10.1115/1.2717232.

[19] Dubois D, Fargier H, Prade H. Possibility theory in constraint satisfaction problems: handling priority, preference and uncertainty. Appl Intell 1996;6:287–309. http://dx.doi.org/10.1007/BF00132735.
[20] Ben-Haim Y. Information-gap decision theory: decisions under severe uncertainty. 2nd ed. Oxford: Academic Press; 2006.
[21] Shafer G. A mathematical theory of evidence, vol. 1. Princeton: Princeton University Press Princeton; 1976.
[22] Bae H-R, Grandhi RV, Canfield RA. Epistemic uncertainty quantification techniques including evidence theory for large-scale structures. Comput Struct 2004;82:1101–12. http://dx.doi.org/10.1016/j.compstruc.2004.03.014.
[23] Helton JC, Johnson JD, Oberkampf WL, Sallaberry CJ. Representation of analysis results involving aleatory and epistemic uncertainty. Int J Gen Syst 2010;39:605–46. http://dx.doi.org/10.1080/03081079.2010.486664.
[24] Limbourg P, De Rocquigny E. Uncertainty analysis using evidence theory–confronting level-1 and level-2 approaches with data availability and computational constraints. Reliab Eng Syst Saf 2010;95:550–64. http://dx.doi.org/10.1016/j.ress.2010.01.005.
[25] Walley P. Statistical reasoning with imprecise probabilities. London: Chapman and Hall; 1991.
[26] Aughenbaugh JM, Paredis CJ. The value of using imprecise probabilities in engineering design. J Mech Des 2006;128:969–79. http://dx.doi.org/10.1115/1.2204976.
[27] Dempster AP. Upper and lower probabilities induced by a multivalued mapping. Ann Math Stat 1967;38:325–39.
[28] Agarwal H, Renaud JE, Preston EL, Padmanabhan D. Uncertainty quantification using evidence theory in multidisciplinary design optimization. Reliab Eng Syst Saf 2004;85:281–94. http://dx.doi.org/10.1016/j.ress.2004.03.017.
[29] Mourelatos ZP, Zhou J. A design optimization method using evidence theory. J Mech Des 2006;128:901–8. http://dx.doi.org/10.1115/1.2204970.
[30] Alyanak E, Grandhi R, Bae H-R. Gradient projection for reliability-based design optimization using evidence theory. Eng Optim 2008;40:923–35. http://dx.doi.org/10.1080/03052150802168942.
[31] Srivastava RK, Deb K. An EA-based approach to design optimization using evidence theory. ACM 2011:1139–46. http://dx.doi.org/10.1145/2001576.2001730.
[32] Salehghaffari S, Rais-Rohani M, Marin EB, Bammann DJ. A new approach for determination of material constants of internal state variable based plasticity models and their uncertainty quantification. Comput Mater Sci 2012;55:237–44. http://dx.doi.org/10.1016/j.commatsci.2011.11.035.
[33] Yang J, Huang H-Z, He L-P, Zhu S-P, Wen D. Risk evaluation in failure mode and effects analysis of aircraft turbine rotor blades using Dempster-Shafer evidence theory under uncertainty. Eng Fail Anal 2011;18:2084–92. http://dx.doi.org/10.1016/j.engfailanal.2011.06.014.
[34] Paris PC, Erdogan F. A critical analysis of crack propagation laws. J Basic Eng 1963;85:528–33. http://dx.doi.org/10.1115/1.3656900.
[35] Tian X, Du H, Sun Z. Metal fatigue crack growth curve fitting method. J Eng Mech 2003;4:136–40. http://dx.doi.org/10.3969/j.issn.1000-4750.2003.04.024 [in Chinese].
[36] Sentz K, Ferson S. Combination of evidence in Dempster-Shafer theory. Albuquerque (New Mexico): Sandia National Laboratories; 2002. vol. SAND2002-0.
[37] Deng LX, Tang HS, Hu CY, Xue ST. Evidence theory and differential evolution for uncertainty quantification of structures. Appl Mech Mater 2012;249–250:1112–8. http://dx.doi.org/10.4028/www.scientific.net/AMM.249-250.1112.
[38] Storn R, Price K. Differential evolution – a simple and efficient heuristic for global optimization over continuous spaces. J Glob Optim 1997;11:341–59. http://dx.doi.org/10.1023/A:1008202821328.
[39] Das S, Suganthan PN. Differential evolution: a survey of the state-of-the-art. Evol Comput IEEE Trans 2011;15:4–31. http://dx.doi.org/10.1109/TEVC.2010.2059031.
[40] Ferson S, Kreinovich V, Ginzburg L, Myers D, Sentz K. Constructing probability boxes and dempster-shafer structures. Albuquerque (New Mexico): Sandia National Laboratories; 2003. vol. SAND2002-4.
[41] Bhachu KS, Haftka RT, Kim NH. Using bootstrap to assess sampling uncertainty in fatigue crack growth life. In: 17th AIAA non-deterministic approaches conf., american institute of aeronautics and astronautics; 2015. http://dx.doi.org/10.2514/6.2015-0662.
[42] Niccolls EH. A correlation for fatigue crack growth rate. Scr Metall 1976;10:295–8. http://dx.doi.org/10.1016/0036-9748(76)90079-X.
[43] Li Y, Wang H, Gong D. The interrelation of the parameters in the Paris equation of fatigue crack growth. Eng Fract Mech 2012;96:500–9. http://dx.doi.org/10.1016/j.engfracmech.2012.08.016.
[44] Iacoviello F. Analysis of stress ratio effects on fatigue propagation in a sintered duplex steel by experimentation and artificial neural network approaches. Int J Fatigue 2004;26:819–28. http://dx.doi.org/10.1016/j.ijfatigue.2004.01.004.
[45] CORTIE MB. The irrepressible relationship between the Paris law parameters. Eng Fract Mech n.d.; 40:2.
[46] Amsterdam E, Grooteman F. The influence of stress state on the exponent in the power law equation of fatigue crack growth. Int J Fatigue 2016;82:572–8. http://dx.doi.org/10.1016/j.ijfatigue.2015.09.013.
[47] Sandberg D, Mansour R, Olsson M. Fatigue probability assessment including aleatory and epistemic uncertainty with application to gas turbine compressor blades. Int J Fatigue 2017;95:132–42. http://dx.doi.org/10.1016/j.ijfatigue.2016.10.001.
[48] Jiang C, Wang B, Li ZR, Han X, Yu DJ. An evidence-theory model considering dependence among parameters and its application in structural reliability analysis. Eng Struct 2013;57:12–22. http://dx.doi.org/10.1016/j.engstruct.2013.08.028.
[49] Xie L, Liu J, Zhang J, Man X. Evidence-theory-based analysis for structural-acoustic field with epistemic uncertainties. Int J Comput Methods 2016:1750012. http://dx.doi.org/10.1142/s0219876217500128.